PCCP

Accepted Manuscript

This is an *Accepted Manuscript*, which has been through the Royal Society of Chemistry peer review process and has been accepted for publication.

Accepted Manuscripts are published online shortly after acceptance, before technical editing, formatting and proof reading. Using this free service, authors can make their results available to the community, in citable form, before we publish the edited article. We will replace this *Accepted Manuscript* with the edited and formatted *Advance Article* as soon as it is available.

You can find more information about *Accepted Manuscripts* in the **Information for Authors**.

Please note that technical editing may introduce minor changes to the text and/or graphics, which may alter content. The journal's standard **Terms & Conditions** and the **Ethical guidelines** still apply. In no event shall the Royal Society of Chemistry be held responsible for any errors or omissions in this *Accepted Manuscript* or any consequences arising from the use of any information it contains.

www.rsc.org/pccp

PCCP

ARTICLE

Graphene oxide–Li+@C₆₀ donor-acceptor composite for photoenergy conversion†

Mustafa Supur,[a] Yuki Kawashima,[a] Kei Ohkubo,[a] Hayato Sakai,[b] Taku Hasobe[b] and Shunichi Fukuzumi*[acd]

An ionic endohedral metallofullerene (Li$^+$@C$_{60}$) with mild hydrophilic nature was combined with graphene oxide (GO) to construct a donor-acceptor composite in neat water. The resulting composite was characterised through UV-Vis and Raman spectroscopy, powder X-ray diffraction, dynamic light scattering measurements and transmission electron microscopy. Theoretical calculations (DFT at B3LYP/6-31(d) level) were also utilized to gain further insight into the composite formation. As detected by electron paramagnetic resonance spectroscopy, photoexcitation of the GO–Li$^+$@C$_{60}$ composite results in electron transfer from GO to the triplet excited state of Li$^+$@C$_{60}$, leading to a photocurrent generation on the OTE/SnO$_2$ electrode.

Introduction

Endohedral metallofullerenes (EMFs), bearing rich chemical and electronic properties determined by the metallic component inside the carbon cage,[1,2] are promising alternatives of empty fullerenes for improving the performance of the current organic optoelectronic devices.[3,4] Accordingly, as one of the recently emerging EMFs, Li$^+$@C$_{60}$ was reported to be a better electron acceptor as compared to its empty predecessor.[5–8] Synthesized by an advanced ion implantation method,[9,10] Li$^+$@C$_{60}$ is the only available ionized-metal-containing EMF, so far. It diverges from the other EMFs with its unique ionic characteristics, that is, while the Li ion is encapsulated inside the carbon cage its counter anion (in this study: PF$_6^-$) stays outside, which simply turns the entire carbon structure into a salt form.[9,11,12] As a result of this polar identity, Li$^+$@C$_{60}$ is expected to present exceptional colloidal characteristics in aqueous environments, different than those of the non-polar, hydrophobic empty fullerenes or the non-ionic EMFs.

On the other hand, graphene oxide (GO), having principally continuous π-conjugation extending in two dimensions, offers new carbon materials for optoelectronic applications.[13–19] Exfoliation of graphite by chemical oxidation introduces oxygen-containing groups on large π-surface of GO, which provide processability in water and non-covalent functionalisation with the conjugate molecules having proper ionic substituents.[20–26] Neutral (non-reduced) GO acts as a good electron donor when combined with suitable electron acceptors during a photoinduced electron-transfer process.[26] However, strong electronic communication through the π-π interactions between the mainly flat π-surface of GO and the planar π-electron acceptors causes very fast charge recombination,[26]

which can reduce the expected performance of optoelectronic devices, essentially based on photodriven charge separation. From this aspect, fullerenes can be ideal electron acceptors because after the photoinduced electron transfer from GO to fullerenes, the fast charge recombination can be delayed by the delocalization of the transferred electron on the spherical π-surface of the fullerenes having geometrically limited electronic interaction with the chiefly flat π-surface of GO as compared to planar electron acceptors while the omni-directional hole migration through the π-conjugations of the two-dimensional GO surface takes place (Fig. S1, ESI). At this point, there are two problems standing against the construction of genuine electron donor-acceptor systems of pristine or metal-containing fullerenes with neutral GO via the non-covalent assembly: First, the extreme hydrophobicity of bucky-balls retards the assembly with GO in the absence of surfactants and/or mediator semiconducting carbon structures in aqueous media at ambient conditions.[27] Second, due to spherical-planar mismatch, π-π interactions between fullerenes and GO is not sufficient for a non-covalent association and an efficient charge separation.[28] Additional intermolecular interactions are required to utilize for a strong binding, providing a fast electron transfer.

Regarding these issues, Li$^+$@C$_{60}$ with ionic characteristics can be suitable components to combine with GO in aqueous environments. Li$^+$@C$_{60}$ emerges as the only fullerene candidate for the assembly with GO in neat water at ambient conditions: Its polar character provides a mild hydrophilicity for the incorporation with GO sheets and the encapsulated Li ion can be readily used for electrostatic interactions with the electron-rich oxygen functionalities on the GO surface for strong binding. In a recent communication, it has been shown that Li$^+$@C$_{60}$ nano-aggregates obtained by a laser irradiation

process have significantly smaller size distribution and more efficient singlet oxygen generation compared to those of C_{60} and C_{70} in an aqueous solution as a result of its mild hydrophilic nature.[29] The role of Li ion inside the fullerene on the binding of $Li^+@C_{60}$ with host molecules containing oxygen-rich moieties through the electrostatic interactions has been comprehensively discussed in previous reports.[30,31] In contrast to the pristine C_{60}, $Li^+@C_{60}$ showed strong interaction with the electron-rich crown ether moieties of host molecules to form robust inclusion complexes, exhibiting the indispensable effect of the Li ion inside the fullerene cage on electrostatic binding.

Complexation of $Li^+@C_{60}$ with anionic porphyrins and phthaloyanines was studied in previous studies.[32–35] Ionic interactions between the encapsulated Li^+ and the anionic substituents were found to be more effective than the π-π interactions between the π-surfaces of fullerene and these flat π-donors. Nevertheless, π-π interactions become operative for the complexation when the host molecule has an appropriate curved π-system to envelope the fullerene cage effectively.[12,36,37] Donor-acceptor systems of $Li^+@C_{60}$ underwent efficient photoinduced electron-transfer processes with long-lived charge separated states due to strong reducing ability of $Li^+@C_{60}$.[38] Photoelectrochemical performances of these donor-acceptor systems of $Li^+@C_{60}$ were significantly improved by the photoinduced electron-transfer events when they were deposited on transparent electrodes.[35,39,40] The photofunctional composites of GO with $Li^+@C_{60}$ have yet to be developed. In this study, we report the characterization and photoinduced electron-transfer and photovoltaic features of a donor-acceptor composite of GO and $Li^+@C_{60}$, the first example of two-dimensional material–EMF combination.

Results and discussion

Characterization of GO–$Li^+@C_{60}$ composite

After applying a few minutes of sonication, $Li^+@C_{60}$ forms well-dispersed, nanometer-size colloids in water, opposite to hydrophobic empty C_{60} (Fig. 1, inset). These nanoparticles give absorption peak at 270 and 351 nm at UV region and a shoulder band at around 460 nm in water (Fig. 1a), which was assigned to the charge-transfer band as a result of intermolecular interactions between the $Li^+@C_{60}$ molecules in the colloids.[29] It is important to note that absorption traits do not change by the variations in concentration. Mean size distribution of $Li^+@C_{60}$ nanoparticles were evaluated to be 140 nm with a size width of 76 nm in water by the dynamic light scattering (DLS) measurements (Fig. S2, ESI). Similarly, mean size distribution does not change significantly by the concentration, which implies the robustness of these colloids. By the addition of GO to the aqueous dispersion of $Li^+@C_{60}$, the absorption peaks at 270 and 351 nm gradually shifts to 250 and 339 nm, respectively, due to possible assembly with GO layers (Fig. 1b). GO was titrated by $Li^+@C_{60}$ in water, as well. This time, the absorption trait of $Li^+@C_{60}$ appeared around 250 and 340 nm shifted to longer wavelengths as the concentration of $Li^+@C_{60}$ was increased (Fig. S3, ESI). The average size distribution of $Li^+@C_{60}$ nanoparticles reduced to 93 nm as well, after the addition of a small amount of GO (Fig. 1c).[41] TEM image confirms the DLS measurements, in which the average size of $Li^+@C_{60}$ clusters on GO is less than 100 nm (Fig. 1d). The nano-aggregates of $Li^+@C_{60}$ with smaller size distribution (30 nm) displayed absorption peaks at the shorter wavelengths (264 and 350 nm) in water in a previous study.[29] Accordingly, the blue shift in the absorption spectra of $Li^+@C_{60}$ nanoparticles in Fig. 1b, observed upon the addition of GO, can be explained by the decrease in the size distribution of $Li^+@C_{60}$. GO surfaces harbour extensive π-conjugations and oxygen functionalities, which apparently provide π-and n-electron-rich environment to the interacting $Li^+@C_{60}$ aggregates in the aqueous environment. Thus, these aggregates 'dissolve' on the GO surfaces through the hydrophobic π-π and n-π interactions.[30,31] Li ion inside the fullerene cage also electrostatically triggers these interactions with the GO surface.[30,31,37] As a result of such interactions, GO surface can host $Li^+@C_{60}$ nanoparticles in water.

To determine the strength of association of $Li^+@C_{60}$ with GO surface in water, the toluene and 1,2-dichlorobenzene
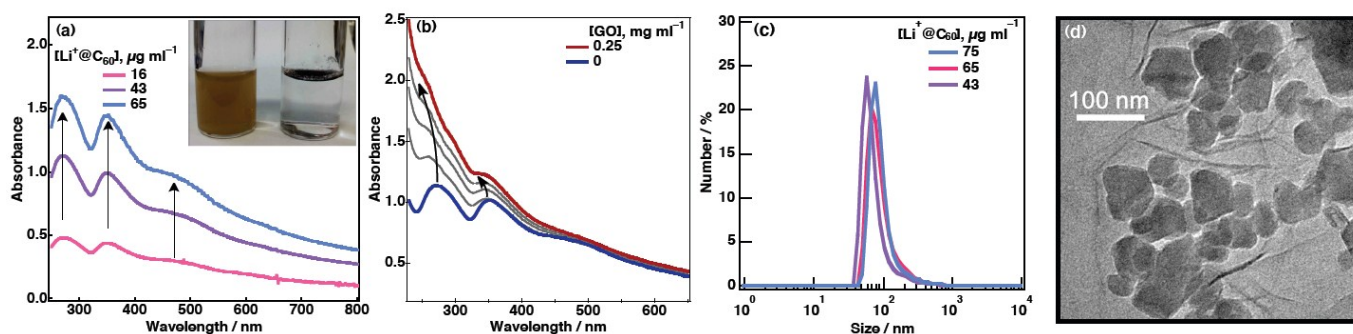
Fig. 1 (a) Absorption spectra of $Li^+@C_{60}$ nanoparticles dispersed in aqueous media at indicated concentrations. Inset: Photographic image of same amount of $Li^+@C_{60}$ dispersed in water (left vial) and empty C_{60} (right vial) floating atop the water taken after several minutes of sonication. (b) Absorption spectral changes upon the titration of 0.20 mg ml^{-1} $Li^+@C_{60}$ aqueous solution by GO aqueous solution. (c) Size distribution diagram of $Li^+@C_{60}$ at indicated concentrations in the presence of 0.018 mg ml^{-1} GO in water. (d) TEM image of GO–$Li^+@C_{60}$ composite obtained from its aqueous solution.

(*o*-DCB) solutions of Li$^+$@C$_{60}$ were treated with the aqueous dispersions of GO (Fig. S5 and S6, ESI). The absorption bands of Li$^+$@C$_{60}$ in these solvents markedly diminished after mixing with GO dispersion. It should be noted that the toluene and *o*-DCB solutions of Li$^+$@C$_{60}$ treated with only water did not give any significant decrease in the absorption spectra of these solutions (Fig. S7, ESI). Therefore, the significant decrease in absorption in the presence of GO is only related to binding of Li$^+$@C$_{60}$ clusters to the GO surface. Estimated by the decline in the absorption peaks, 2.0 mg GO in water can extract 0.042 (2.1%, m/m) and 0.053 mg (2.7%, m/m) Li$^+$@C$_{60}$ from toluene and *o*-DCB solutions, respectively. The solubility of Li$^+$@C$_{60}$ in *o*-DCB is about 10 times higher in toluene.[42] As its solubility decreases in the organic media the amount of Li$^+$@C$_{60}$ extracted by GO in aqueous environment increases. Therefore, the binding of Li$^+$@C$_{60}$ to GO is most probably related to the desolvation of fullerene cages[30,43] at distinct regions of the GO surfaces where strong interaction occurs.

Powder X-ray diffraction (PXRD) showed that Li$^+$@C$_{60}$ clusters have face-centered cubic (fcc) structure in the solid state (Fig. S8, ESI).[44] The slight shifts in the corresponding peaks of Li$^+$@C$_{60}$ were observed in the PXRD patterns compared to those of C$_{60}$. This can be due to the effect of the counter anions of Li$^+$@C$_{60}$ (PF$_6^-$) on the cluster structure.

Dispersed Li$^+$@C$_{60}$ nanoparticles lead to increase in the average *d*-spacing between GO layers from 8.6 Å to 9.4 Å as detected by the shift of the denoted peak[45] in PXRD patterns
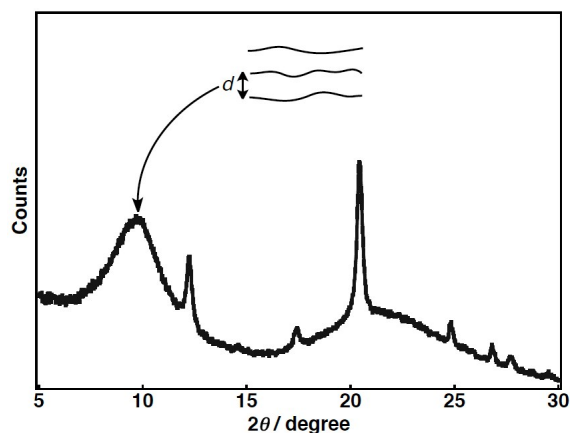
Fig. 2 Powder X-ray diffraction patterns of dried GO–Li$^+$@C$_{60}$ composites obtained from dispersion in water.
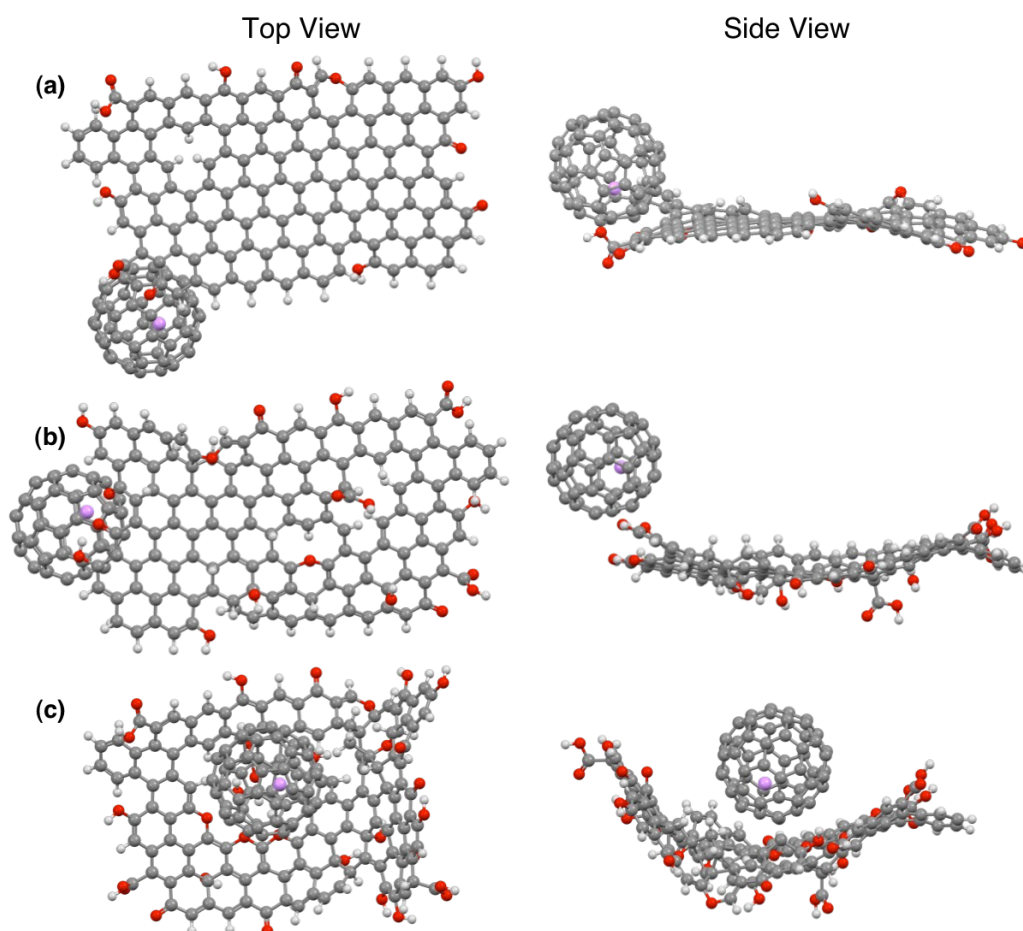
Fig. 3 Top (left) and side (right) views of optimized structures showing the binding sites of Li$^+$@C$_{60}$ with the hypothetical portions of GO having 10% (a), 15% (b), and 23% (c) oxygen percentage by mass (calculated by DFT at the B3LYP/6-31(d) level of theory).

of GO–Li$^+$@C$_{60}$ composite in the solid state (Fig. 2). Li$^+$@C$_{60}$ clusters maintain the fcc structure in these composites, as they conserve the corresponding peaks in Fig. 2. This indicates that incorporation of Li$^+$@C$_{60}$ cages into the GO layers is limited. Incorporation of Li$^+$@C$_{60}$ clusters into the GO layers was also verified by the shift of stretching mode of Li$^+$@C$_{60}$ from 1459 to 1461 cm^{-1} in the Raman spectrum in the presence of GO (Fig. S9, ESI). Hence, the solid state of composite forms the stacks of the GO layers between which the fullerenes are partially hosted.

The hosting sites for Li$^+$@C$_{60}$ on the GO surface was investigated in light of density functional (DFT) methods at the . As shown in Fig. 3, three hypothetical portions of GO, respectively having 10%, 15%, and 23% oxygen composition by mass, were optimized in the presence of a Li$^+$@C$_{60}$ molecule. Graphene surfaces were functionalized by the most common oxygen functionalities observed after chemical oxidation process.[46] There is no knowledge about the location and the density of oxygen groups.[46] The initial oxidation should take place on the edges of the graphite flakes rather than the their inner regions because of the strong stacking of graphene layers in the graphite. In agreement with this argument, oxygen groups were first distributed only on the edges of the GO portion with 10% oxygen content. As the oxygen content increases by the further oxidation process, the inner regions of the portions were also decorated with the oxygen functionalities.[46] Hydrogen composition was fixed to around 2% by mass for each hypothetical portions of GO to see the effect of oxygen impurities on the honeycomb structure and on the binding of Li$^+$@C$_{60}$ to these surfaces. In each GO portion, Li$^+$@C$_{60}$ sites where the most of the oxygen functional groups are accumulated, regardless of their type (ether, ketone, carboxyl, etc.). Li ion takes position inside the fullerene cage with a noteworthy proximity to the electron-rich oxygen atoms as a result of electrostatic interactions as noticed in the side views of optimized structures (Fig. 3). Disposition of the fullerenes on the edge of GO surface in Figures 3a and 3b also indicates that electrostatic interactions of Li ion with the boundary oxygen functionalities are much stronger than π-π interactions between the carbon cage and flat honeycomb structure. This suggests that the effect of π-π interactions on binding is limited in these portions. Accumulation of more oxygen atoms causes the loss of flatness of the honeycomb structure as shown in Fig. 3c. As result of this, there exist curved regions (pockets) on the GO surface. Such pockets apparently maintain n-π interactions with oxygen groups and π-π interactions with the conveniently curved π-conjugations, by which the Li$^+$@C$_{60}$ molecules can be effectively hosted. Short d-spacing in the presence of Li$^+$@C$_{60}$ (Fig. 2) can be explained by such curved regions on GO where fullerene cages inserted as illustrated in Scheme 1. Li$^+$@C$_{60}$ molecules place into the already existing pockets so that the average distance between the GO layers does not change significantly. Although the DFT calculations portray the complexation phenomenon at the molecular level, the similar discussion for the hosting

behaviour of the GO surface for the nanoparticles of Li$^+$@C$_{60}$ through the same interactions is applicable.
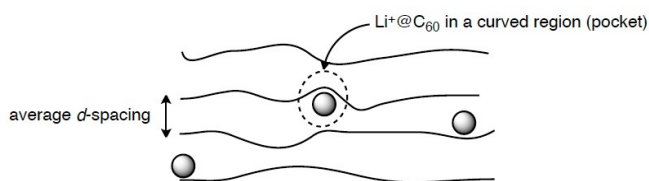
Scheme 1. Illustration of hosting of Li$^+$@C$_{60}$ molecule in the curved regions of GO layers.

Photoinduced events and photovoltaic features of GO–Li$^+$@C$_{60}$ composite

The free energy change of proposed photoinduced charge separation via the excited states of Li$^+$@C$_{60}$ (ΔG_{CS}) in the GO–Li$^+$@C$_{60}$ composite was calculated according to eqn (1),[47]

$$\Delta G_{CS} = e(E_{ox} - E_{red}) - E_S$$

where E_{ox} is the first oxidation potential of GO, E_{red} is the first one-electron reduction of Li$^+$@C$_{60}$, and E_S is the lowest excited states of Li$^+$@C$_{60}$. Energy levels of singlet (^{1}Li$^+$@C$_{60}$*) and triplet excited states (^{3}Li$^+$@C$_{60}$*) of Li$^+$@C$_{60}$ were calculated to be 1.94 and 1.53 eV, respectively.[6] E_{red} and E_{ox} of Li$^+$@C$_{60}$ and GO were previously reported as 0.14[5,6] and 0.88 V vs. SCE,[26] respectively. Hence, the photoinduced electron transfer from GO to ^{1}Li$^+$@C$_{60}$* and ^{3}Li$^+$@C$_{60}$* is feasible with driving forces of 1.20 and 0.79 eV, respectively.

Photoinduced charge separation in the GO–Li$^+$@C$_{60}$ composite was observed by using electron paramagnetic resonance (EPR) spectroscopy, in which the formation of radical ions was detected upon the photoexcitation at 77 K in water (Fig. 4a). Photoexcitation of GO–Li$^+$@C$_{60}$ composite at 4 K revealed the spin state of the charge-separated state to be a triplet with the EPR signal at g = 4.18, suggesting that charge separation is realized by electron transfer from GO to ^{3}Li$^+$@C$_{60}$* (Fig. S10, ESI). The EPR signal at 77 K appeared within a few seconds upon excitation and started to decay when the light was switched off (Fig. S11, ESI). Such a fast charge separation results from the strong binding of Li$^+$@C$_{60}$ to the GO surface through oxygen moieties. On the other hand, intermolecular electron transfer from free Li$^+$@C$_{60}$ molecules to the GO is likely to occur through the long-lived ^{3}Li$^+$@C$_{60}$* in the same environment. From the decay of EPR signal intensity, the lifetime of the charge-separated state was estimated to be 250 s at 77 K (Fig. 4a, inset). Slow charge recombination can be due to the hole migration between the GO layers[26] in addition to the delocalization of the radical anion (Li$^+$@C$_{60}$•⁻) on the spherical π-system of fullerene.

Photoinduced events based on EPR measurements were summarized in the energy-level diagram (Fig. 4b). Intersystem crossing yields ^{3}Li$^+$@C$_{60}$* from ^{1}Li$^+$@C$_{60}$*, which provides sufficient driving force for electron transfer in GO–Li$^+$@C$_{60}$ due to the lower energy level of the charge-separated state.
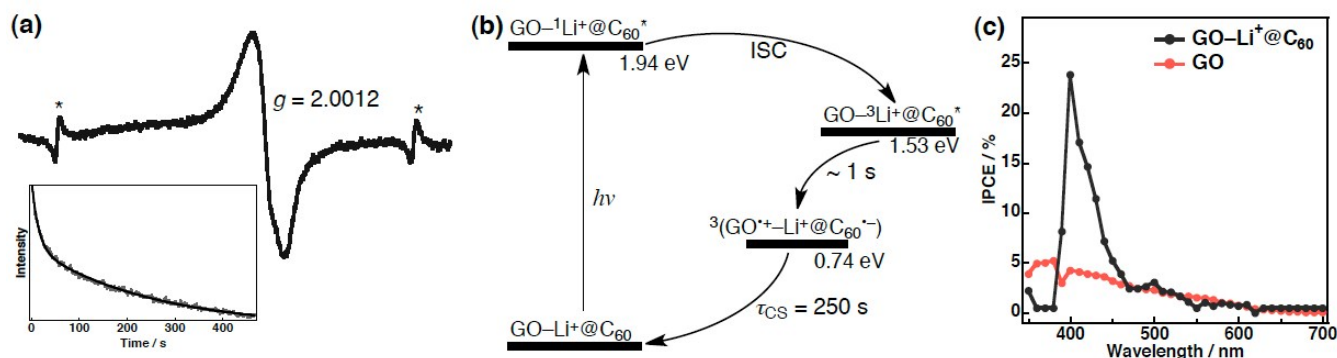
Fig. 4 (a) EPR spectrum of GO–Li$^+$@C$_{60}$ composite in deaerated water showing the radical ion formation at 77 K observed after photoirradiation. Asterisks denote the Mn^{2+} markers. Inset: Decay profile of EPR signal intensity of radical ion pair of GO–Li$^+$@C$_{60}$ composite in water obtained after switching off the photoirradiation at 77 K. (b) Energy-level diagram showing the photoinduced events of GO–Li$^+$@C$_{60}$ composite. (c) Photocurrent action spectra of OTE/SnO$_2$–(GO)$_n$ and OTE/SnO$_2$–(Li$^+$@C$_{60}$)$_n$. Electrolyte: 0.5 M LiI and 0.01 M I$_2$ in MeCN–PhCN (3 : 1 v/v).

To determine the response of the GO–Li$^+$@C$_{60}$ composite towards the photocurrent generation, it was deposited on an optically transparent electrode (OTE) of nanostructured SnO$_2$ (OTE/SnO$_2$–(GO–Li$^+$@C$_{60}$)$_n$) and a series of photocurrent action spectra were compared with those of only GO deposited on OTE of SnO$_2$ (OTE/SnO$_2$–(GO)$_n$) in the electrolyte system. The maximum value of incident photon-to-photocurrent efficiency (IPCE) of OTE/SnO$_2$–(GO)$_n$ was only 5% at 380 nm while OTE/SnO$_2$–(GO–Li$^+$@C$_{60}$)$_n$ gave an IPCE value of 24 % at 400 nm (Fig. 4c). The maximum IPCE value of OTE/SnO$_2$–(Li$^+$@C$_{60}$)$_n$ was also estimated to be only 5% (at 425 nm) in a previous study.[39] Apparently, there is no contribution of the individual components to the enhancement of the IPCE in the composite. Therefore, the remarkable enhancement of IPCE together with the photo-voltage response of OTE/SnO$_2$–(GO–Li$^+$@C$_{60}$)$_n$ (Fig. S12, ESI) reflect that the photocurrent generation in this composite system was initiated by a photoinduced electron-transfer process from (GO)$_n$ to (Li$^+$@C$_{60}$)$_n$. After the photoinduced charge-separation process takes place, the reduced Li$^+$@C$_{60}$ injects (0.14 V vs. SCE) electron into the conduction band of SnO$_2$ (0.2 V vs. SCE), whereas the oxidized GO undergoes electron-transfer reduction with I$^-$/I$_3^-$ in the electrolyte solution.[39]

Conclusions

In conclusion, a new donor-acceptor composite consisting of GO and Li$^+$@C$_{60}$ was constructed. Electrostatic interactions of Li ion with the electron-rich oxygen functionalities on the GO surface were found to be very essential for the association with Li$^+$@C$_{60}$ rather than the π-π interactions with the flat π-conjugations of GO. Incorporation of Li$^+$@C$_{60}$ into GO layers leads to photoinduced electron transfer under photoirradiation, which markedly enhances the photocurrent generation of the OTE/SnO$_2$ electrode loaded with GO–Li$^+$@C$_{60}$ composites. The present results indicate that this new composite can be a promising photoenergy conversion material for the prospective optoelectronic devices.

Experimental section

Materials

Graphene oxide (GO; as dispersions in water: 2.0 and 4.0 mg ml^{-1}; Sigma-Aldrich) and [Li$^+$@C$_{60}$]PF$_6^-$ (98% purity, Idea International Co. Ltd.) were used as received. Purification of water (18.2 MΩ cm) was performed with a Milli-Q system (Millipore, Direct-Q 3 UV). GO and Li$^+$@C$_{60}$ were extensively sonicated before measurements.

Instruments

Steady-state absorption measurements were recorded on a Hewlett Packard 8453 diode array spectrophotometer. Dynamic light scattering (DLS) measurements were carried out using a Zetasizer Nano S (Malvern Instruments Ltd., USA). The DLS instrument used in this work has a range between 0.6 nm and 6000 nm, and thereby any structures over this limit cannot be detected. Transmission electron micrograph (TEM) measurements were recorded on Tecnai spirit (FEI company) by applying a drop of the sample to a copper grid. TEM images were recorded on a transmission electron microscope an accelerating voltage of 120 kV for imaging. Powder X-ray diffraction (PXRD) patterns were recorded by a Rigaku Ultima IV. Incident X-ray radiation was produced by Cu X-ray tube, operating at 40 kV and 40 mA with Cu Kα radiation of 1.54 Å. A scanning rate was 4° min^{-1} from 4° to 50° in 2θ. Raman spectra of were obtained using a JASCO NR-1800 with a 514.5 nm Ar laser. PXRD and Raman spectroscopy samples were prepared by drying for overnight. Density-functional theory (DFT) calculations were performed on a COMPAQ DS20E computer. The structures of corresponding complexes were optimized to a stationary point on the Born–Oppenheimer potential-energy surface. Geometry optimizations were carried out using the B3LYP functional and 6-31G (d) basis set,[48] as implemented in the Gaussian 03 program Rev. C.02. Graphical outputs of the computational results were generated with the

Gauss View software program (ver. 3.09) developed by Semichem, Inc. The electron paramagnetic resonance (EPR) spectra were taken on a JEOL X-band spectrometer (JES-RE1XE) under photoirradiation with a high-pressure mercury lamp (USH-1005D) through a water filter focusing the sample cell in the EPR cavity at 4 or 77 K. Electrophoretic electrode deposition was performed using a Power Pac HV (Bio-Rad). Photoelectrochemical measurements were carried out in a standard two-compartment cell consisting of a working electrode, a Pt wire gauze counter electrode. A KEITHLEY 2400 was used for recording *I-V* characteristics and photocurrent generation density under an AM 1.5 simulated light source (OTENTO-SUN II, Bunkoh Keiki Co., LTD). For the IPCE measurements, a monochromator (SM-25, Bunkoh Keiki Co., LTD) was introduced into the path of the excitation beam (150 W Xenon lamp, Bunkoh Keiki Co., LTD) for the selected wavelength. The lamp intensity at each wavelength was determined using a Si photodiode (Hamamatsu Photonics S1337-1010BQ) and corrected.

Acknowledgements

Notes and references

a Department of Material and Life Science, Graduate School of Engineering, Osaka University, ALCA and SENTAN, Japan Science and Technology Agency (JST), Suita, Osaka 565-0871, Japan

b Department of Chemistry, Faculty of Science and Technology, Keio University, Yokohama, Kanagawa 223-8522, Japan

c Department of Bioinspired Science, Ewha Womans University, Seoul 120-750, Korea

d Faculty of Science and Engineering, Meijo University, ALCA and SENTAN, Japan Science and Technology Agency (JST), Nagoya, Aichi 468-0073, Japan

† Electronic Supplementary Information (ESI) available: Additional figures (Fig. S1 to S12). See DOI: 10.1039/b000000x/

1   A. A. Popov, S. Yang and L. Dunsch, *Chem. Rev.*, 2013, **113**, 5989–6113.

2   H. Cong, B. Yu, T. Akasaka and X. Lu, *Coord. Chem. Rev.*, 2013, **257**, 2880–2898.

3   A. Hirsch, *Nat. Mater.*, 2010, **9**, 868–871.

4   R. B. Ross, C. M. Cardona, D. M. Guldi, S. G. Sankaranarayanan, M. O. Reese, N. Kopidakis, J. Peet, B. Walker, G. C. Bazan, E. Van Keuren B. C. Holloway and M. Drees, *Nat. Mater.*, 2009, **8**, 208–212.

5   S. Fukuzumi, K. Ohkubo, Y. Kawashima, D. S. Kim, J. S. Park, A. Jana, V. M. Lynch, D. Kim and J. L. Sessler, *J. Am. Chem. Soc.*, 2011, **133**, 15938–15941.

6   Y. Kawashima, K. Ohkubo and S. Fukuzumi, *J. Phys. Chem. A*, 2012, **116**, 8942–8948.

7   S. Fukuzumi, K. Ohkubo, F. D'Souza and J. L. Sessler, *Chem. Commun.*, 2012, **48**, 9801–9815.

8   Y. Kawashima, K. Ohkubo and S. Fukuzumi, *J. Phys. Chem. A*, 2013, **117**, 6737–6743.

9   S. Aoyagi, E. Nishibori, H. Sawa, K. Sugimoto, M. Takata, Y. Miyata, R. Kitaura, H. Shinohara, H. Okada, T. Sakai, Y. Ono, K. Kawachi, K. Yokoo, S. Ono, K. Omote, Y. Kasama, S. Ishikawa, T. Komuro and H. Tobita, *Nat. Chem.*, 2010, **2**, 678–683.

10   X. Lu, L. Feng, T. Akasaka and S. Nagase, *Chem. Soc. Rev.*, 2012, **41**, 7723–7760.

11   H. Ueno, K. Kokubo, Y. Nakamura, K. Ohkubo, N. Ikuma, H. Moriyama, S. Fukuzumi and T. Oshima, *Chem. Commun.*, 2013, **49**, 7376–7378.

12   H. Ueno, T. Nishihara, Y. Segawa and K. Itami, *Angew. Chem., Int. Ed.*, 2015, **54**, doi: 10.1002/anie.201500544

13   K. P. Loh, Q. Bao, G. Eda and M. Chhowalla, *Nat. Chem.*, 2010, **2**, 1015–1024.

14   D. Chen, H. Feng and J. Li, *Chem. Rev.*, 2012, **112**, 6027–6053.

15   I. V. Lightcap and P. V. Kamat, *Acc. Chem. Res.*, 2013, **46**, 2235–2243.

16   H. Chang and H. Wu, *Energy Environ. Sci.*, 2013, **6**, 3483–3507.

17   Q. Tang, Z. Zhou and Z. Chen, *Nanoscale*, 2013, **5**, 4541–4583.

18   J. Yuan, J. Zhu, H. Bi, X. Meng, S. Liang, L. Zhang and X. Wang, *Phys. Chem. Chem. Phys.*, 2013, **15**, 12940–12945.

19   P. Yu, X. Wen, Y.-R. Toh, Y.-C. Lee, K.-Y. Huang, S. Huang, S. Shrestha, G. Conibeer and J. Tang, *J. Mater. Chem. C*, 2014, **2**, 2894–2901.

20   Q. Su, S. Pang, V. Alijani, C. Li, X. Feng and K. Müllen, *Adv. Mater.*, 2009, **21**, 3191–3195.

21   A. Wojcik and P. V. Kamat, *ACS Nano*, 2010, **4**, 6697–6706.

22   J. Geng and H.-T. Jung, *J. Phys. Chem. C*, 2010, **114**, 8227–8234.

23   Z. D. Liu, H. X. Zhao and C. Z. Huang, *PLoS ONE*, 2012, **7**, e50367. doi: 10.1371/journal.pone.0050367

24   S. Srinivasan, S. H. Je, S. Back, G. Barin, O. Buyukcakir, R. Guliyev, Y. Jung and A. Coskun, *Adv. Mater.*, 2014, **26**, 2725–2729.

25   S. Roy, D. K. Maiti, S. Panigrahi, D. Basak and A. Banerjee, *Phys. Chem. Chem. Phys.*, 2014, **16**, 6041–6049.

26   M. Supur, K. Ohkubo and S. Fukuzumi, *Chem. Commun.*, 2014, **50**, 13359–13361.

27   V. C. Tung, J.-H. Huang, I. Tevis, F. Kim, J. Kim, C.-W. Chu, S. I. Stupp, J. Huang, *J. Am. Chem. Soc.*, 2011, **133**, 4940–4947.

28   M. Barrejon, M. Vizuete, M. J. Gomez-Escalonilla, J. L. G. Fierro, I. Berlanga, F. Zamora, G. Abellan, P. Atienzar, J.-F. Nierengarten, H. Garcia and F. Langa, *Chem. Commun.*, 2014, **50**, 9053–9055.

29   K. Ohkubo, N. Kohno, Y. Yamada and S. Fukuzumi, *Chem. Commun.*, 2015, **51**, doi: 10.1039/c5cc01885d

30   M. Supur, Y. Kawashima, K. R. Larsen, K. Ohkubo, J. O. Jeppesen and S. Fukuzumi, *Chem.–Eur. J.*, 2014, **20**, 13976–13983.

31   M. Supur, Y. Kawashima, Y.-X. Ma, K. Ohkubo, C.-F. Chen and S. Fukuzumi, *Chem. Commun.*, 2014, **50**, 15796–15798.

32   K. Ohkubo, Y. Kawashima and S. Fukuzumi, *Chem. Commun.*, 2012, **48**, 4314–4316.

33   Y. Kawashima, K. Ohkubo, M. Kentaro, and S. Fukuzumi, *J. Phys. Chem. C*, 2013, **117**, 21166–21177.

34 Y. Kawashima, K. Ohkubo, H. Okada, Y. Matsuo and S. Fukuzumi, *ChemPhysChem*, 2014, **15**, 3782–3790.

35 Y. Kawashima, K. Ohkubo, V. M. Blas-Fernando, H. Sakai, E. Font-Sanchis, J. Ortiz, F. Fernandez-Lazaro, T. Hasobe, A. Sastre-Santos and S. Fukuzumi, *J. Phys. Chem. B*, 2015, **119**, doi: 10.1021/jp102966x

36 S. Hitosugi, K. Ohkubo, R. Iizuka, Y. Kawashima, K. Nakamura, S. Sato, H. Kono, S. Fukuzumi and H. Isobe, *Org. Lett.*, 2014, **16**, 3352–3355.

37 M. Yamada, K. Ohkubo, M. Shionoya and S. Fukuzumi, *J. Am. Chem. Soc.*, 2014, **136**, 13240–13248.

38 Y. Kawashima, K. Ohkubo and S. Fukuzumi, *Chem.–Asian J.*, 2014, **10**, 44–54.

39 K. Ohkubo, Y. Kawashima, H. Sakai, T. Hasobe and S. Fukuzumi, *Chem. Commun.*, 2013, **49**, 4474–4476.

40 K. Ohkubo, Y. Kawashima, K. Mase, H. Sakai, T. Hasobe and S. Fukuzumi, *J. Porphyrins Phthalocyanines*, 2014, **18**, 982–990.

41 Normally, the mean size of high amount of GO dispersed in water was calculated as 230 nm by DLS measurements (Fig. S4, ESI). To clearly observe the change in the size distribution of only $Li^+@C_{60}$ nanoparticles by the addition of GO, the concentration of GO in Fig. 1c was set to be too low.

42 We assumed that $Li^+@C_{60}$ has solubility similar to parental C_{60} in these solvents. For the solubility of C_{60} in various solvents, see: R. S. Ruoff, D. S. Tse, R. Malhotra and D. C. Lorents, *J. Phys. Chem.*, 1993, **97**, 3379–3383 and Ref 1.

43 A. Hosseini, S. Taylor, G. Accorsi, N. Armaroli, C. A. Reed and P. D. W. Boyd, *J. Am. Chem. Soc.*, 2006, **128**, 15903–15913.

44   J. C. Scanlon and L. B. Ebert, *J. Phys. Chem.*, 1993, **97**, 7138–7140.

45 For the assignment of corresponding peak in Fig. S8, ESI and the average values of *d*-spacing between GO layers, see: Refs 24 and 26.

46 A. Bagri, C. Mattevi, M. Acik, Y. J. Chabal, M. Chhowalla and V. B. Shenoy, *Nat. Chem.*, 2010, **2**, 581–587.

47 A. Weller, *Z. Phys. Chem.*, 1982, **133**, 93–98.

48 W. J. Hehre, L. Radom, P. V. R. Schleyer and J. A. Pople, Ab Initio Molecular Orbital Theory; Wiley: New York 1986.